

On The Orbital Evolution of Jupiter Mass Protoplanet Embedded in A Self-Gravity Disk

Hui Zhang^{1,2}, Chi Yuan¹, D.N.C. Lin^{3,4} and David C.C. Yen^{1,5}

ABSTRACT

We performed a series of hydro-dynamic simulations to investigate the orbital migration of a Jovian planet embedded in a proto-stellar disk. In order to take into account of the effect of the disk's self gravity, we developed and adopted an **Antares** code which is based on a 2-D Godunov scheme to obtain the exact Riemann solution for isothermal or polytropic gas, with non-reflecting boundary conditions. Our simulations indicate that in the study of the runaway (type III) migration, it is important to carry out a fully self consistent treatment of the gravitational interaction between the disk and the embedded planet. Through a series of convergence tests, we show that adequate numerical resolution, especially within the planet's Roche lobe, critically determines the outcome of the simulations. We consider a variety of initial conditions and show that isolated, non eccentric protoplanet planets do not undergo type III migration. We attribute the difference between our and previous simulations to the contribution of a self consistent representation of the disk's self gravity. Nevertheless, type III migration cannot be completely suppressed and its onset requires finite amplitude perturbations such as that induced by planet-planet interaction. We determine the radial extent of type III migration as a function of the disk's self gravity.

Subject headings: accretion disks — hydrodynamics — methods: numerical — planetary systems: formation — planetary systems: protoplanetary disks

¹Institute of astronomy and astrophysics, Academia Sinica ,Taipei

²Department of Astronomy,NanJing University, Nanjing

³UCO/Lick Observatory, University of California, Santa Cruz

⁴Kavli Institute of Astronomy and Astrophysics, Peking University,Peking

⁵Department of Mathematics, Fu Jen Catholic University, Taipei

1. Introduction

More than 200 planets have been discovered around nearby solar-type stars. Their kinematic properties are characterized by diversities in their mass, period, eccentricity, and physical radius. An important dynamical process which may have led to these properties is protoplanets' migration due to their tidal interaction with their nascent disks (Lin & Papaloizou 1993; Papaloizou & Terquem 2006). The progenitor cores of gas giant planets undergo type I migration due to a torque imbalance between different regions of the disks where they are embedded (Goldreich & Tremaine 1980; Ward 1984). After they have acquired sufficient mass to open a gap near their orbit, gas giant planets' orbital evolution is locked to that of the disk gas through a type-II migration (Lin & Papaloizou 1986). But under some circumstances, the gap may be partially cleared and the disk gas which leak through this region can induce the gas giants to undergo runaway (type III) migration (Masset & Papaloizou 2003, hereafter MP).

All of these process can relocate protoplanets far from their birth place. The rapid time scale for type-I migration (Ward 1997; Tanaka,Takeuchi & Ward 2002) poses a challenge to the formation of gas giant planets (Thommes & Murray 2006; Ida & Lin 2007). But several potential retardation mechanisms have been proposed. They include variation in the surface density and temperature gradient (Masset,D'Angelo & Kley 2006b), intrinsic turbulence in the disk (Laughlin,Steinacker & Adams 2004; Nelson & Papaloizou 2004), and non-linear radiative and hydrodynamic feedbacks (Masset *et al.* 2006a). If these cores are formed in the turbulent free dead zone (Gammie 1996), self-induced unstable flow (Koller 2004; Li *et al.* 2005; de Val-Borro *et al.* 2007) would reduce the efficiency of type I migration by an order of magnitude (Dobbs-Dixon *et al.* 2007, in preparation).

Type-II migration has been invoked as a mechanism for the formation of close-in gas giants (Lin,Bodenheimer & Richardson 1996). Both 1D (Lin & Papaloizou 1986) and 2D (D'Angelo *et al.* 2006) simulations have shown that before disk gas mass decays to the value comparable to the planet mass, the planet migrates with (unperturbed) disk accretion on a viscous diffusion time scale and when disk gas mass is comparable to the planet mass, only a fraction of the total (viscous plus advective) angular momentum flux transported by the disk gas (which is assumed to be independent of the disk radius) is utilized by the planet in its orbital evolution (Ivanov,Papaloizou & Polnarev 1999). The inclusion of type-II migration in the planet formation models has yield a mass-period distribution which is similar to that observed (Ida & Lin 2004a,2004b, 2005, 2007).

Type III migration is driven by a strong corotation torque very near the planet (Ida *et al.* 2000, MP). The time scale for this process is much shorter than both type I and type II migration. If it commonly occurs, type III migration would greatly erase any signature in the

dynamical structure of planetary systems from the disk initial surface density distribution of their nascent disks. Due to its dramatic effects, type III migration has been extensively studied over the past few years (Ogilvie & Lubow 2006). This process can only be maintained if there is an uninterrupted flow across the planet’s orbit so that saturation of the corotation resonances can be avoided. Masset and Papaloizou(2003) show that the radial motion of a rapidly migrating planet can indeed be self sustained, *i.e.* its motion leads to the fresh supply to the corotation region which provides a torque to induce further migration. Ida *et al.* 2000 demonstrated a similar effect for planetary migration induced by residual planetesimals. They suggest that the critical condition for the onset of this process is that the mass of the residual planetesimals contained within the feeding zone (with a half width up to a few times that of the Roche radius) must exceed that of the planet. The results of the hydrodynamic simulations (MP) also show that a planet would undergoes runaway migration in disk regions with $\delta m \geq M_{planet}$, where δm is the mass of the disk gas in the planet’s co-orbital region. For a Jupiter-mass, this requirement implies a mass ratio between the entire disk and the central star to be $\mu \equiv \frac{M_d}{M_\star} \gtrsim 0.02$.

In such disks, the effect of the disk self gravity is important, especially in the determination of the torque applied to the gas in the planet’s co-orbital region by that in other regions of the disk. But in the previous numerical simulations, the effect of the disk’s self gravity has been neglected. In this paper, we develop a new numerical scheme which takes the effect of disk self gravity into account. With this scheme, our main objectives are to examine the conditions under which type III migration is launched and sustained. In §2, we provide a description of our computational method and model parameters.

The simulation of MP showed that type III migration is spontaneous excited in relatively massive disks. We consider two limiting initial conditions. In the first set of simulations, we consider the emergence of an isolated planet on a circular orbit. In the core accretion scenario, the growth of gas giants occur on time scales much longer than the synodic time scale in most nearby disk regions such that the stream lines can adjust adiabatically. In the second set of simulations, we introduce a set of “dynamically quiescent” initial conditions by gradually increasing the planet’s mass over many orbits and the initial angular velocity of planet is not exact Keplerian(The centrifugal force will balances the gravity both from center star and the whole gas disk) so that the disk gas can adjust to its tidal potential of the planet and attain a dynamical equilibrium. During this transition stage, the semi major axis of the planet is artificially held fixed. This “quiet-start” prescription is introduced to minimize the impulse felt by the gas at the onset of the simulation. With this initial condition, we carried out several series of simulations to determine the dependence of the disk flow and planet’s migration on the numerical resolution and the degree of the disk self gravity. In §3, we present the results of these simulations.

The “quiet-start” models provide a test on whether type-III migration may be spontaneously launched under the optimum conditions as indicated by the numerical simulation by MP. They also provided a powerful analytic argument to suggest that it can be sustained once type-III migration is initiated. Ida *et al.* (2000) found that this process may need an “initial push” due to some large perturbations. In the second series of simulations, we consider this possibility by introducing an initial jolt as a trigger for type-III migration. One potential mechanism for this impulsive perturbation is close encounter between two proto-planet (Zhou *et al.* 2005). In §4, we present the simulated results of the “initial-push” models. Finally, we summary our results and discuss their implications in §5.

2. Physical and Numerical Model

2.1. Physical model

Following conventional procedures, we simulate the dynamical response of a gas disk around a star which is located at the origin of the coordinates. We constructed a 2D numerical hydrodynamic scheme to solve the continuity and momentum equations, neglecting the effect of any explicit viscosity. We place a protoplanet which is initially embedded in the disk with a circular orbit around the central star. In order to avoid some well-known problems (see below) at the inner boundary (close to the central star), we solve the governing equations in the Cartesian coordinate.

The vertically averaged continuity equation for the disk gas is given by

$$\frac{\partial \sigma}{\partial t} + \frac{\partial(\sigma u_x)}{\partial x} + \frac{\partial(\sigma u_y)}{\partial y} = 0 \quad (1)$$

The equations of motion in the Cartesian coordinates are

$$\frac{\partial(\sigma u_x)}{\partial t} + \frac{\partial(\sigma u_x^2)}{\partial x} + \frac{\partial(\sigma u_x u_y)}{\partial y} = -\frac{\partial P}{\partial x} - \sigma \frac{\partial \Phi}{\partial x} \quad (2)$$

$$\frac{\partial(\sigma u_y)}{\partial t} + \frac{\partial(\sigma u_x u_y)}{\partial x} + \frac{\partial(\sigma u_y^2)}{\partial y} = -\frac{\partial P}{\partial y} - \sigma \frac{\partial \Phi}{\partial y} \quad (3)$$

where P is pressure and Φ is the gravity potential of the star-planet-disk system, which includes the softened potential of central star (Φ_s), softened potential of the planet (Φ_p), potential of the disk itself (Φ_d) and indirect potential (Φ_i) due to the acceleration of origin by planet and disk. The softened potential of central star is given by $\Phi_s = -\frac{GM_\odot}{\sqrt{x^2+y^2+\epsilon_{star}^2}}$ and the softened potential of planet is $\Phi_p = -\frac{GM_p}{\sqrt{(x-x_p)^2+(y-y_p)^2+\epsilon_p^2}}$ where ϵ_{star} and ϵ_p are the

soften length to central star and planet respectively. In all the models presented here, we adopt ϵ_p is half of the planet’s Roche radius. **Fig.1** shows the rotation curves of the disk when we adopt different ϵ_{star} . During our simulations it is 0.1 in units where the initial semi major axis of the planet is unity (in some other simulations we reduce it to 0.05 and find little difference).

2.2. Numerical Method

The **Antares** code we have developed is adopted in the calculations. It is a 2-D Godunov code based on the exact Riemann solution for isothermal or polytropic gas, featured with non-reflecting boundary conditions. The details of this code has described elsewhere(Yuan & Yen 2005).

Full self-gravity of the disk is calculated by FFT. We assume the disk gas has an isothermal equation of state and we don’t add any explicit viscosity in the simulation. There is however some numerical viscosity associated with our computational scheme. Extensive tests indicate that the magnitude of artificial viscosity is equivalent to $\alpha < 10^{-4}$. Shock is treated with standard von Neuman prescription. For the orbit of planet we adopt RK78 to integrate it.

2.3. Computational mesh configuration and domain

In many models, the planet’s orbit undergoes extensive decays. A natural system to solve the governing equations is the polar coordinates. But, the axial symmetric of the disk flow is broken by the presence of the planet. The inner boundary conditions can only be an approximate function of the disk radius along well inside the orbit of the planet. Although the Fargo prescription provides a resolution for this technical challenge over some regions of the disk, it is nonetheless difficult to achieve extend the computational domain to very small R_{inner} with Polar coordinates because the computational time $T_{com} \sim R_{inner}^{-3/2}$.

A Cartesian coordinate system introduces some advantages over the polar coordinates. It is easy to achieve high resolution without the bottle-neck in the azimuthal direction. It is also straight forward to calculate self-gravitating effect with FFT. During some of our simulations we adopt a 512×512 grid, while in some high resolution cases it increases to 1024×1024 . To carry out the calculation, however, a softening length ϵ_{star} is assigned to the central star, where ϵ_{star} is one order smaller than the length unit. Computational domain is from -2.5 to 2.5 in both x,y direction. Primary star locates at the origin where $x=0$ and $y=0$.

To avoid symmetric problem of the four corners we extend the disk to $R=5$ and assume the area outside the computational square ($x \times y = 5 \times 5$) will stay constant (See **Fig.2**) during the evolution, while the gravity is taken account all over the area within $R \leq 5$.

2.4. Computational Units

For numerical convenience we set gravitational constant $G = 1$, solar mass $M_\odot = 1$ and the radius of planet’s initial orbit $R_0 = 1$, where $R_0 = 5.2AU$. The unit of time is $1/2\pi$ of the planet’s initial orbit period P_0 . Most of our simulations are carried out over a period of $1000P_0$. Since the unit of density σ_0 drops out of the equations of motion, we can normalize it to any specified density.

2.5. Initial Conditions

At the beginning of evolution, the disk surface density is set to be uniform. We adopt 4 different initial surface density: $\Sigma_0 = 0.6 \times 10^{-3}, 0.9 \times 10^{-3}, 1.2 \times 10^{-3}, 1.5 \times 10^{-3}$. The mass of thinnest disk is about $0.012M_\odot$ which is about the minimum mass of solar nebula, while the thickest one is about $0.03M_\odot$. The angular velocity of the gas $v_\theta = r\Omega_g$ is slightly different from the Keplerian velocity since the flow is in a centrifugal balance with both the softened gravity of the star and self-gravity of the disk (when self-gravitating effect is included) such that $v_\theta = \Omega_g r = \sqrt{\frac{rGM_\odot}{r^2 + \epsilon^2} + r f_{sg}}$. In disks with an isothermal equation of state and a homogenous surface density distribution, the pressure gradient effect does not contribute to the initial azimuthal speed. The initial radial velocity of gas is set to be 0. These initial disk conditions do not take into account the gravitational perturbation by the planet.

The initial azimuthal velocity of the planet is also set to balance the gravity of the central star and that of the disk. The initial location of planet is at $(x=1, y=0)$. In the simplest models, planet’s initial mass is 10^{-3} ($1M_J$) and is fixed during the evolution. This approach introduces a gravitational impulse which can strongly perturb the stream line, especially near the planet’s orbit.

For “quiet-start” models, we adjust the initial velocity to set up a dynamical equilibrium in which the planet’s orbit is circular and the stream lines are closed. To do so, we adopt an negligible initial mass for the planet (3×10^{-7} or equivalently $0.1M_\oplus$). We specify the planet’s growth rate to be 3% during every orbit period until it grows to $1M_J$ within the first 250 fixed circular orbit periods. With this prescription the planet gains mass through

adiabatic growth and the disk has enough time to make smooth response. Before the planet is launched, we further adjusted the azimuthal speed of the planet so that it regains a circular orbit despite the presence of the gas.

2.6. Boundary conditions

We adopt non-reflection boundary condition, that means we do wave decomposition at each boundary and set all the waves that propagate inward to computational domain to be zero. So the wave can only propagate outward and we had assume the area is constant outside boundary, that makes the wave absorbed at the boundary. While the boundary isn't closed to mass flow, gas may flows through the boundary freely according to the equation of motion. The area outside the boundary is assume to be uniform and maintain the initial condition without evolution. The details of this boundary condition had been described elsewhere(Godon 1996).

3. Simulations of flow with a quiet starts

A series of hydrodynamic simulations had been performed(see **Table 1**). At first, we consider a series of simplest models(S1-S4). In these models, the numerical resolution is relatively low (512×512), the prescription for self-gravitating and quiet-start effects are NOT included. We specify the planet's mass to one Jupiter mass and test four different surface density of disk.

From the lowest to the highest surface density $\Sigma = 0.6 \times 10^{-3}, 0.9 \times 10^{-3}, 1.2 \times 10^{-3}$ and 1.5×10^{-3} (in units of solar mass divides by the square of the planet's initial radius). The results show that the migration rate is proportional to the surface density of disk. In the limit that the disk's surface density is higher than 1.2×10^{-3} , a very rapid migration occurs(See **Fig 3**).

This result is in agreement with that obtained by MP. For the critical model, the disk-to-primary mass ratio ($\pi \Sigma R_d^2 / M_*$) is a little above 0.01 and planet-to-primary mass ratio is 0.001. According to the criterion specified by MP, this set of parameter is at the boundary of the 'runaway domain', so the migration curve shows a critical property. When the surface density becomes higher, the model parameters are totally in the 'runaway area' and the migration is much faster. MP had suggested that this rapid migration is due to the planet's co-rotation torque being consistently replenished by the disk gas which flow through the planet's orbit. We present detailed analysis for the high resolution models to support with

conjecture.

3.1. Resolution

The above simulation show that the torque density is most intense near the orbit of the protoplanet, especially within its Roche radius. With the adopted mass ratio, the planet’s Roche radius is about 0.069 in our dimensionless unit. For the relatively low resolution (512×512) models, the width of each grid is $\delta x = \delta y = 0.01$. In these models, there are only 7 grids within planet’s Roche radius. Torques associated with large m resonances can not be well resolved in this limited resolution and the under-resolved torques may lead to some unreasonable effect.

In principle, the nearly symmetric flow pattern within the Roche radius is expected to lead to large cancellation of the net torque applied by the circum planetary disk on the planet at its center. But the direct consequence of inadequate numerical resolution is that the gas accumulated in the Roche lobe will generate large artificial fluctuations in the magnitude of the torque applied to the planet which cannot be easily cancelled. In Figure 4, we show that the ratio (Γ) of the tidal torque (on the planet) by the gas within planet’s Roche lobe to the tidal torque (on the planet) by the gas within the entire disk. The rapid oscillations of this ratio is clearly shown. This inadequate resolution of the flow pattern introduces an inconsistency in which the planet and the gas flow within it’s Roche lobe are dragged along by each other.

The issue with resolving the flow within the Roche lobe is clearly illustrated by the sensitive dependence of the migration rate on the softening length for the planet’s potential (Nelson & Benz 2003a,2003b; Cresswell & Nelson 2006). In the low-mass limit where the Roche radius is smaller, the lack of resolution introduces even more severe problems for both type-I and type-III migration because they are strongly determined by the flow close to the planet. Inadequate resolution is less serious for type-II migration in which case a gap is clearly formed and the gas in planet’s Roche lobe is depleted. Nevertheless, inadequate resolution may also lead to artificial diffusion of gas into the gap. Figure 4 shows large fluctuation in the magnitude of Γ after the gap has formed (at $\sim 100P_0$) in the low resolution models. There is also gas flow across planet’s Roche lobe where torque imbalance is amplified by the coarsely resolved mesh. Leakage of fresh gas into the planet’s co-orbital region can also sustain a gradient in the potential vorticity and suppression of corotation saturation (Masset *et al.* 2006a) which may reduce the efficiency of type II migration from disk gas accretion(Crida & Morbidelli 2007). The corotation torque scales with the gradient of the

potential vorticity(Goldreich & Tremaine 1979;Ward 1991,1992):

$$\Gamma_C \propto \Sigma \frac{d \log \frac{\Sigma}{B}}{d \log r}, \quad (4)$$

For a sufficiently smooth,monotonic transition of surface density from Σ_i to Σ_o the vorticity logarithmic gradient is therefore(Masset *et al.* 2006a):

$$\frac{d \log \frac{\Sigma}{B}}{d \log r} = \frac{r}{\lambda} \log \frac{\Sigma_o}{\Sigma_i} (a + b \frac{H^2}{\lambda^2}), \quad (5)$$

where a and b are constants of numerical functions of r of unity that depend on the shape of the surface density profile. H is the scale hight of the disk and $\lambda \ll r$ is the length scale of the density transition, which are both constant too.

3.2. Convergence tests

In order to highlight the problems introduced by the inadequate numerical resolution, we carry out several high resolution (1024×1024) simulations. The upper panel of Figure 4 shows that the fluctuation in the magnitude of Γ declined greatly after the gap has formed (at $\sim 100P_0$) in the high resolution models. A combination in the reduction of artificial numerical viscosity and adequately resolved torque greatly reduces the artificial torque imbalance on the planet due to the gas within the Roche lobe (also see D'Angelo *et al.* 2005). Consequently, the planet's migration is also significantly reduced.

Figure 5 shows the planet's orbital evolution for simulations with different resolutions. In two separate sets of initial surface densities, other than a modest initial radial decay during the epoch of gap formation, type III (runaway) migration is essentially eliminated. The dichotomy between these models (S3 and H2) is particularly dramatic for the models with sufficiently high disk mass that the type III migration is spontaneously launched in the low-resolution simulations.

Another useful diagnostic is the surface density distribution. In Figures 6 and 7 we show the density evolution of models S3 and H2. Figure 7 clearly shows the presistent presence of gas in the 'horse shoe' region and an un-axisymmetric structure at the edge of the gap. The high- resolution simulation in Figure 7 shows a sharper disk edge and more clearly defined wave pattern than the lower-resolution simulation. The high resolution simulations require several months of CPU time. Although, our simulations are carried out with greater resolution than most existing calculations, we are not yet able to achieve higher resolution and test numerical convergence at this stage.

3.3. Self-gravity

The results in the previous subsection illustrate the contribution to the torque on the planet by the gas within the Roche lobe. Although this amount of material in this region is small compared with the mass of the planet, the gravity between it and the planet is strong due to their proximity. In fact, a fraction of this gas actually resides in a disk around and is gravitationally attached to the planet. As we have indicated above that the net torque on the planet by the gas in the proto-planetary disk is expected to be mostly cancelled and its mass should share the torque from the rest of the disk with the planet.

In most of the published numerical simulations, the effect of the disk’s self gravity is not included. This approximation introduces an inconsistent gravitational field felt by the planet and by the gas which shares its orbit. In this section, we consider the effect of self-gravity in models $SG1 \sim SG4$ and $QG1 \sim QG4$. Due to limited computational resources, these models are simulated with low resolutions (512x512). Although inadequate resolution continues to plague the proper determination of the tidal torque, we use these models to demonstrate that a self-consistent treatment of the disk self gravity couples the flow within the planet’s Roche lobe to it and reduces the rate of type-III migration.

Results in Figure 3 show that the migration slows down slightly (a few percent) in a low- Σ models (SG1 and SG2) when self-gravitating effect is included (similar results are obtained by Nelson & Benz 2003a,b). However in the high- Σ models SG3 and SG4, the difference brought by the self-consistent treatment of the disk’s self gravity is much more pronounced. At $10^3 P_0$, the migration in case SG3 slows down by almost 50% relatively to that in model S3 where the effect of the disk’s self gravity is neglected. And more importantly, the ‘runaway migration’ doesn’t occurs when sufficiently high values of Σ which did lead to ‘runaway migration’ in a non-self-gravitating disk.

We note that, in all models with identical Σ distribution, the planet have the same orbital decay rate regardless whether the effect of self gravity is included. This similarity is probably due to the slightly artificial impulse initial conditions adopted here. In these series of simulations, gas in the disk is forced to respond to the planet’s gravity for the first time at the onset of the computation. This initial impulse leads to large potential vorticity gradient which ensures a strong contribution from the corotation resonances. Under some circumstance, the planet migrates inwards by a sufficiently large increment, a fresh supply of disk gas with new values of potential vorticity is brought to the co-orbital region of the planet such that the further migration is promoted. For most disks, however, the replenishment of fresh disk material is inadequate to self sustain the run away migration.

The difference between these two series of models become more pronounced after the

gap formation. In this limit, replenishment of the co-orbital region is quenched. As gas librates on horse-shoe orbits, any initial potential vorticity gradient is erased such that the contribution from the corotation resonance become saturated and weakened.

In Figure 8, we plot the Σ distribution for the self gravitating model SG3. In this model, the clearing of the gap strongly enhances the effect of self gravity near the boundary of the gap. Although the Q -value of the disk near the planet’s orbit is initially $Q \gg 1$, but the clearing and accumulation of gas beyond the gap leads to a local $Q \sim 2$ near the outer edge of the gap. With such a low Q -value at a relatively sharp disk edge, un-axisymmetric gravitational (Papaloizou & Lin 1989) and shearing (Balmforth & Korycansky 2001; Li *et al.* 2005; de Val-Borro *et al.* 2007) may be excited. These instabilities can significantly reduce the migration speed (Koller *et al.* 2003, Dobbs-Dixon *et al.* in preparation).

Finally, the treatment of self gravity closely ties together the planet and the gas within its Roche lobe. With a self consistent treatment of the gas self gravity, the interaction between the planet and a significant fraction of the gas within its Roche lobe becomes a binding rather than dispersive force. The self gravity of the gas beyond the gap region can only start to dominate the torque after the flow has established an equilibrium pattern such that the gas in the co-orbital region migrate together with the planet as integral parts.

4. Isolated protoplanet versus perturbed system

The results in Figure 3 suggest a transition in the protoplanet-disk tidal interaction from being dominated by corotation resonances to their saturation as gas in the co-orbital region is being cleared out. We consider two limiting possibilities: a “quiet” and an “impulsive” start.

4.1. Quiet start

According to the core-accretion scenario, the most favorable location for the first generation of gas giants to form is near the snow line (Ida & Lin 2004). Since the growth time scales for their progenitor cores is sensitively dependent on their disk environment and their gas accretion is a runaway process, the first gas giants are likely to form in isolation over many dynamical time scales (Pollack *et al.* 1996). In principle, the disk can adjust adiabatically to the perturbation due to the emergence of the gas giants. This expectation provides the rationale for a set of simulations with a “quiet start” (for a description of the quiet-start prescription, see section 2).

We adopt a quiet start in 8 models (See **Table 1**), four of them include the effect of self-gravitating while the others do not. With a quiet start, a clear gap is formed near the planet’s orbit such that the corotation resonance is saturated from the onset. Since the disk is able to establish a dynamical equilibrium through adiabatic adjustments, the impulsive perturbation at the epoch of planet release is minimized. In all cases, the migration rate is greatly suppressed and type III migration is halted. This result is consistent with the MP conjecture that unsaturated corotation resonances are responsible for inducing the type III migration. (See **Fig.9**).

The introduction of the quiet start algorithm reduces the differential motion between the protoplanet and the disk gas at this proximity and enhances the gravitational interaction between them. Consequently, the effect of self-gravity becomes more pronounced earlier than it does in models without the quiet start (See **Fig.10**). With a quiet start and self gravity of the disk, we minimize inconsistencies of the numerical simulations for planets grow adiabatically in isolation. In all models with this combination, runaway migration is suppressed.

4.2. Impulsive initial perturbation

Although, run away migration is unlikely to be initiated spontaneously, it can nevertheless be self sustained by mobile planets. Following the framework in MP’s analysis, let us suppose the planet has already acquired some initial velocity and is moving inward relative to the disk gas. The “first move” can be the result of close-encounters between two gas giants or a strong dynamical perturbation by some external stellar perturbation.

In order to consider such a possibility, we simulated 5 additional models which the disk and planetary parameters of model Q3. At the end stage of Q3, a Jupiter-mass planet (A) is centered in a severely depleted gap and its migration is essentially halted, — *i.e.* the planet-disk system has established an equilibrium structure. At this instant of time, we assume there is another planet (B) which enters into a close encounter with planet A with an impact parameter $0.5R_{roche}$ (where R_{roche} is the Roche radius of planet A). The duration of the close encounter is brief ($\sim P_0/20$). In the five test models (IQ1-IQ5), we adopt 5 different mass of planet B (See **Table.2**). The results are shown in **Fig.11**.

The simulated results of models IQ1-IQ3 indicate that Planet A is not significantly perturbed by close encounters with a much less massive planet B. In each of these models, planet A move inward slightly and then retain the dynamical equilibrium and its migration is halted. In model IQ4, planet B is sufficiently massive to induce planet A to undergo a

ten percent decay in its semi major axis (See Fig.11). But planet A manages to open a sufficiently clear gap that the corotation resonance become saturated. Thereafter, runaway migration is also halted in model IQ4 but after migration over a substantial radial extent.

Shortly after the scattering event, planet A’s eccentricity acquires a finite amplitude (Fig.12). In models IQ1-IQ3, planet A acquires eccentricities smaller than the ratio of Roche radius to its semi major axis. Thus, planet A avoids direct contact with a substantial amount of disk gas. In model IQ4, planet A’s modest eccentricity shortly after the perturbation results in its periodic excursion into the disk region beyond the gap. In principle, the disk gas is periodically fed to the planet and the condition for run away migration is satisfied. (Although the corotation and Lindblad resonances provide modest flux of angular momentum transport per synodic period, these contributions accumulate in time.) But the tidal interaction between the disk gas and the planet through the corotation resonance also leads to intense eccentricity damping (Goldreich & Tremaine 1980; Goldreich *et al.* 2004) on time scale comparable to or shorter than that for the runaway migration time scale (with the possible exception of model IQ5 in which the planet’s run away migration is launched).

Once the planet’s eccentricity is suppressed, gas flow through the co-orbital region, especially through the planet’s Roche lobe, can only be self sustained with a sufficiently large radial velocity. Our models show that finite amplitude perturbation excites a positive feedback: 1) planet migrate inward leads to disk gas flowing pass it, 2) corotation resonance takes away the planet’s angular momentum and induces it to further migrate inwards. The comparison between models IQ3-IQ5 shows that the recoil speed of planet A increases with the mass of planet B. The critical amplitude of the perturbation needed to launch this self-sustained migration is that the supply into co-orbital region, during the horseshoe orbits’ libration time scale, must be comparable to or larger than the mass of the planet (MP).

In model IQ5, the planet undergoes run-away migration over an extensive radial distance. In the co-moving frame of the planet, the disk gas travels from inner to outer regions of the disk and remove angular momentum from it through the corotation resonance (or equivalently, the gas is being scattered to large distances by the planet). The disk-planet interaction is greatly amplified during the passage of the gas through planet’s Roche lobe where the imbalance of the torque is a direct consequence of a self-sustained potential vorticity gradient. In comparison to model Q3, we find that the disk’s self-gravity, as a global and indirect effect, can only overwhelm the local flow through the planet’s Roche lobe when its vicinity is severely depleted and the impact of the initial impulse has decayed or is suppressed.

We interpret the results in models IQ3-IQ5 in terms of torque due to the corotation resonance from the gas inside the planet’s radius. In the discussion on models S3 and H2, we have already indicated that inadequate resolution can introduce spurious torque imbalance

which may drive type III migration. But we also showed in models SG3 and Q3 that both self gravity and a quiet start can suppress type III migration even when the flow is simulated with inadequate resolution. In these cases, the torque imbalance may be further reduced in simulations with more a refined numerical resolution. In comparison with the results of model IQ1-IQ3, the launch of type III migration in models IQ4 and IQ5 is due to a physical effect rather than a numerical flaw. In these models, the planet’s orbital evolution is dominated by the local torque (include those hasn’t been well resolved) when there is sufficient mass near it. **Fig.13** shows the surface density distribution within planet A’s vicinity after the scattering event. The figures a,b,c and d correspond to the cases IQ1,IQ3,IQ4 and IQ5 respectively. *a.* For small perturbation, density profile within the vicinity of planet doesn’t change much and planet A remains its equilibrium(IQ1 & IQ2). *b.* Gas starts to flood into planet A’s vicinity(The gray lines) short after relatively large perturbation and evokes a potential vorticity gradient. However the gas depletes soon after $25P_0$ (The light green lines) so there is no runaway migration and the planet come back to its equilibrium shortly after perturbation(IQ3). *c.* In IQ4 gas takes about $400P_0$ to deplete(The red lines) and the corotation resonance which associates with vorticity gradient was suppressed then. Planet A had undergone fast migration through a extensive radial region, however the migration is suppressed finally since it can not self-sustained the vorticity gradient. *d.* Large radial perturbation allows planet A self-sustain the vorticity gradient in its vicinity, and as a result of that, planet A’s keep losing angular momentum through the corotation resonance and under goes a run-away migration.

5. Summary and discussions

In this paper, we are motivated to consider the origin and evolution of the type-III (run away) migration. This process is thought to be important for Saturn mass planets which may have formed in disks more massive than the minimum mass nebula. We are particularly interested in two issues: 1) whether this process can occur spontaneously for isolated gas giants which formed through gas accretion onto solid cores on time scales much longer than the dynamical time scale in the disk; and 2) whether type-III migration can be self-sustained by a planet which is strongly perturbed by a close encounter with another planet.

We performed a series of numerical simulations to investigate the orbit evolution of a embedded planet. In models S1-S4 which are of the simplest settings in which a Jupiter-mass planet is inserted into an isothermal disk with a constant surface density. In all cases, migration occurs with a speed which is an increasing function of the disk mass. For disks with more than twice the mass of the minimum mass nebula model, the planet undergoes

type III migration.

Although these results are intriguing, we identify three technical issues which may have led to an artificial outcome for the numerical simulations. In an attempt to carry out a convergence analysis, we note that our low-resolution models (comparable in resolution to most existing simulations) contain only 14×14 mesh grids across the planet’s Roche lobe. Insufficient numerical resolution introduces an artificial torque imbalance especially for the gas flow within the planet’s Roche lobe. When this region is intruded by a disk flow, unphysical net torque is generated spuriously. This torque induces the planet to rapidly migrate. When the flow through the identical disks is simulated with twice the resolution in each direction, the torque imbalance of the flows through the Roche lobe and the rate of planetary migration are greatly reduced. These studies suggest that under-resolved simulations may lead to spurious runaway migrations. In the work presented here, we cannot yet demonstrate that we have reached numerical convergence. It will require more powerful computational algorithms and tools to determine the condition for adequate resolution.

The second technical problem which plagues many existing numerical simulations is an inconsistent treatment of the disk self gravity. In the computation of the force acting on the planet, both the axisymmetric and the non-axisymmetric components of the gravity from the disk gas are applied to the planet along with the host star’s gravity. But in the evaluation of the equation of motion of the disk gas, the disk’s own contribution to the gravity is not included. In low-mass disks, the discrepancy introduced by this approximation is negligible. But, in disks more massive than the minimum mass nebula, this inconsistency can lead to a differential motion between the planet and the disk gas near its orbit. The absence of disk self gravity also modifies the effect of angular momentum transport across both the corotation and Lindblad resonances (Goldreich & Tremaine 1982). A comparison between models S3 and SG3 show that the extent of radial migration after a time span of $10^3 P_0$ would be reduced by a factor of two if the effect of the self gravity of the disk is included. Nevertheless, runaway migration is not totally suppressed by the disk’s self gravity. Type III migration is spontaneously launched in model SG4 which is also gravitationally unstable—at the out part of the disk $Q \sim 1$. But in general, a self consistent treatment of the disk self gravity can significantly slow down the type-III migration rate.

The last technical issue we have considered is the artificial initial conditions. In the standard models S1-S4, the initial motion of the disk gas is set up for Keplerian velocities so that it is in a centrifugal balance with the host star’s gravity. At the onset of the simulation, the introduction of the planet’s gravity induces a strong perturbation to the flow pattern. Consequently, the disk gas can easily enter into the Roche lobe of the planet and intensely exchange angular momentum with the planet. Since the initial potential vorticity gradient

is preserved, corotation resonance is artificially intensified at the onset of the simulation (see models SG1-SG4). In the formation of the first-generation, isolated gas giants, the planets’ mass grows over many dynamical time scales. The dynamics and structure of the disk flow adjacent to the planet adjust adiabatically through gap formation and modification of stream lines. In an attempt to simulate this gradual process, we carried out two series of models (Q1-Q4) with a “quiet-start” initial condition. In these models, the mass of the planet is increased gradually over $250P_0$. In the first series, models Q1-Q4, we neglect the effect of the disk’s self gravity whereas in the second series, models QG1-QG4, the effect of the disk self gravity is fully implemented. In both sets of simulations, a quiet start greatly suppress the corotation resonance and hence the planet’s type-III migration. In all cases, (including the models for a very massive disk Q4 and QG4), type III migration ceased.

While the quiet start initial condition is justified for the first-generation, isolated planets, it is not appropriate for strongly perturbed planets. A large fraction of all known gas giants reside in multiple planet systems. Indeed the formation of first-generation planets promotes the build up of the cores and the formation of gas giants planet beyond the outer edge of the gap around them (Bryden *et al.* 2000). Despite the gaseous background, if these planets are formed with an initial separation less than about three times the sum of their Roche radius, dynamical instabilities can induce them to undergo close encounters well before the gas is depleted (Zhou, Lin & Sun 2007). In order to investigate these perturbation in the presence of the disk gas, we simulated models IQ1-IQ5. Our results show that the runaway migration of a Jupiter mass planet can be triggered by its close encounters with another planets more massive than Saturn. Immediately after the encounter, the eccentricity of the planet is excited such that it can undergo radial excursion beyond the edge of the gap. Although this motion enables the disk gas to venture into the planet’s Roche lobe, their interaction through the corotation resonances damps the eccentricity faster than directly induce type-III migration. However, the initial impulse may be self sustained by the modest radial motion of the planet. In the co-moving frame of the planet, the disk gas moves across its orbit, sustains a potential vorticity gradient, and induces the planet to undergo type-III migration over large radial distances.

In an attempt to account for the wide eccentricity distribution among the extra solar planets, several authors have consider the possibility of dynamical instability in multiple planet systems (Papaloizou & Terquem 2001; Juric & Tremaine 2007; Chatterjee, Ford, & Rasio 2007; Zhou, Lin & Sun 2007). The time scale for the onset of dynamical instability is a rapidly increasing function of the planet’s separation. In many simulations, compact systems of planets are imposed initially such that they become dynamically unstable on time scale much shorter than both the growth time scale for gas giant planets and the gas-depletion time scale (a few Myr) in their nascent disks. For example, Juric and Tremaine (2007) present several

models to show that, dynamical relaxation in a gas free environment can induce the medium separation between gas giant planets to increase from <5 to >12 within 10^{5-6} yr. The results presented here suggest that close encounters triggered by dynamical instabilities, if frequently occurred prior to the depletion of the disk gas, would launch proto gas giant planets on type-III migration either towards their host stars or the outer edge of their nascent disks. Either outcome may not be compatible with the observed mass-period distribution of extra solar planets. An alternative scenario is the formation of first generation gas giants strongly modified their neighborhood by opening up planetesimal gaps at several Hill's radius from themselves (Zhou & Lin 2007) as well as wide gas gaps (Bryden *et al.* 2000). With moderate large separations, the growth time scale for dynamical instabilities may be lengthened by one or more orders of magnitude. Provided the dynamical instability leads to close encounters between gas giants after the depletion of the disk gas, it is possible for most of them to remain in the proximity of their birth place. Quantitative verification of this conjecture will be presented elsewhere.

6. Acknowledgement

We thank Drs Hui Li and Jilin Zhou for useful conversation. The work is in parts supported by a grant from National Basic Research Program of China (2007CB4800), Natural Science Foundation of China (10403004), National Science Council, Taiwan NSC94-2752-M-001-002-PAE, NASA (NAGS5-11779, NNG04G-191G, NNG06-GH45G), JPL (1270927), and NSF(AST-0507424).

REFERENCES

- Balmforth, N. J., Korycansky, D.G. 2001, MNRAS, 326, 833
- Bryden, G., R?yczka, M., Lin, D.N.C., & Bodenheimer, P. 2000, ApJ, 540, 1091
- Chatterjee, S., Ford, E.B., & Rasio, F.A. 2007, ApJ, submitted
- Cresswell, P., & Nelson, R.P. 2006, *a*, 450, 833
- Crida, A., & Morbidelli, A. 2007, MNRAS, 377, 1324
- D'Angelo, G., Bate, M.R., & Lubow, S.H. 2005, MNRAS, 358, 316
- D'Angelo, G., Lubow, S.H., & Bate, M.R. 2006, ApJ, 652, 1698

- de Val-Borro, M., Artymowicz, P., D'Angelo, G., & Peplinski, A., 2007, *in press*
- Gammie, C.F. 1996, *ApJ*, 462, 725
- Godon, P. 1996, *MNRAS*, 282, 1107
- Goldreich, P., & Tremaine, S. 1979, *ApJ*, 233, 857
- Goldreich, P., & Tremaine, S. 1980, *ApJ*, 241, 425
- Goldreich, P., & Tremaine, S. 1982, *ARA&A*, 20, 249
- Goldreich, P., Lithwick, Y., & Sari, Re'em, 2004, *ApJ*, 614, 497
- Ida, S., & Lin, D.N.C. 2004, *ApJ*, 604, 388
- Ida, S., & Lin, D.N.C. 2004, *ApJ*, 616, 567
- Ida, S., & Lin, D.N.C. 2005, *ApJ*, 626, 1054
- Ida, S., & Lin, D.N.C. 2007, *ApJ*, submitted
- Ida, S., Bryden, G., Lin, D. N. C., & Tanaka, H. 2000, *ApJ*, 534, 428
- Ivanov, P.B., Papaloizou, J.C.B., & Polnarev, A.G. 1999, *MNRAS*, 307, 79
- Juric, M., & Tremaine, S. 2007, *ApJ*, submitted
- Koller, J., Li, H., & Lin, D.N.C. 2003, *ApJ*, 596, 91
- Koller, J. 2004, Thesis (PhD). RICE UNIVERSITY, Source DAI-B 65/02, p.789
- Laughlin, G., Steinacker, A., & Adams, F. C. 2004, *ApJ*, 608, 489
- Li, H., Li, S.T., Koller, J., Wendroff, B.B., Liska, R., Orban, C.M., Liang, E.P.T., & Lin, D.N.C. 2005, *ApJ*, 624, 1003
- Lin, D.N.C. & Papaloizou, J.C.B. 1986, *ApJ*, 309, 846
- Lin, D.N.C. & Papaloizou, J.C.B. 1993, in *Protostars and planets III*, ed. E.H. Levy & J.I. Lunine (Tucson: Univer. Arizona Press), 749
- Lin, D.N.C., Bodenheimer, P., & Richardson, D.C. 1996, *Nature*, 380, 606
- Masset, F.S. & Papaloizou, J.C.B. 2003, *ApJ*, 588, 494
- Masset, F. S., Morbidelli, A., Crida, A. & Ferreira, J. 2006, *ApJ*, 642, 478

- Masset, F. S., D'Angelo, G. & Kley, W. 2006, *ApJ*, 652, 730
- Nelson, A. F. & Benz, W. 2003, *ApJ*, 589, 556
- Nelson, A. F. & Benz, W. 2003, *ApJ*, 589, 578
- Nelson, R., & Papaloizou, J.C.B. 2004, *MNRAS*, 350, 849
- Ogilvie, G.I. & Lubow, S.H. 2006, *MNRAS*, 370, 784
- Papaloizou, J. C. B., & Lin, D. N. C. 1989, *ApJ*, 344, 645
- Papaloizou, J. C. B & Terquem, C. 2001, *MNRAS*, 325, 221
- Papaloizou, J. C. B & Terquem, C. 2006, *RPPh*, 69, 119
- Pollack, J. B., Hubickyj, O., Bodenheimer, P., Lissauer, J. J., Podolak, M., & Greenzweig, Y. 1996, *Icarus*, 124, 62
- Tanaka, H., Takeuchi, T., & Ward, W. R. 2002, *ApJ*, 565, 1257
- Thommes, E. W., & Murray, N. 2006, *ApJ*, 644, 1214
- Ward, W.R. 1984, in *Planetary rings*, ed. R. Greenberg and A. Brahic, (Tucson: University of Arizona Press), pp. 660-684
- Ward, W.R. 1991, *Lunar & Planet. Sci.*, 22, 1463
- Ward, W.R. 1992, *Lunar & Planet. Sci.*, 22, 1491
- Ward, W.R. 1997, *Icarus*, 126, 261
- Yuan, C., & David, C.C. Yen 2005, *JKAS*, 38, 197
- Zhou, J.L., & Lin, D.N.C. 2007, *ApJ*, in press
- Zhou, J.L., Aarseth, S.J., Lin, D.N.C., & Nagasawa, M. 2005, *ApJ*, 631, 85
- Zhou, J.L., Lin, D.N.C., & Sun, Y.S. 2007, *ApJ*, in press

Table 1. Simulations in this paper

Case	Disk Surface Density	Resolution	Self-gravity	Quiet start	Runaway migration
S1	0.6×10^{-3}	512×512	No	No	No
S2	0.9×10^{-3}	512×512	No	No	No
S3	1.2×10^{-3}	512×512	No	No	Yes
S4	1.5×10^{-3}	512×512	No	No	Yes
H1	0.6×10^{-3}	1024×1024	No	No	No
H2	1.2×10^{-3}	1024×1024	No	No	No
SG1	0.6×10^{-3}	512×512	Yes	No	No
SG2	0.9×10^{-3}	512×512	Yes	No	No
SG3	1.2×10^{-3}	512×512	Yes	No	No
SG4	1.5×10^{-3}	512×512	Yes	No	No
Q1	0.6×10^{-3}	512×512	No	Yes	No
Q2	0.9×10^{-3}	512×512	No	Yes	No
Q3	1.2×10^{-3}	512×512	No	Yes	No
Q4	1.5×10^{-3}	512×512	No	Yes	No
QG1	0.6×10^{-3}	512×512	Yes	Yes	No
QG2	0.9×10^{-3}	512×512	Yes	Yes	No
QG3	1.2×10^{-3}	512×512	Yes	Yes	No
QG4	1.5×10^{-3}	512×512	Yes	Yes	No

Table 2. Simulations of Impact

Case	Encounter planet mass	Runaway migration
IQ1	$5M_{earth}$	No
IQ2	$15M_{earth}$	No
IQ3	$50M_{earth}$	No
IQ4	$100M_{earth}$	Critical
IQ5	$300M_{earth}$	Yes

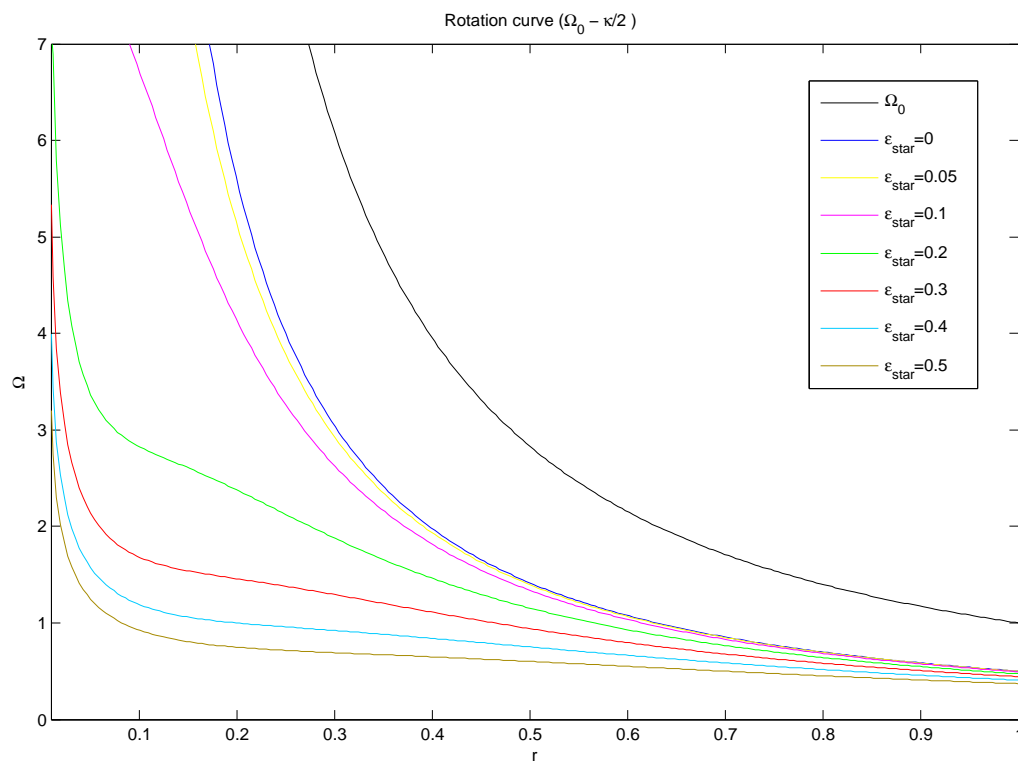


Fig. 1.— Rotation curves of disk. We test the rotation curves when different ϵ_{star} is adopted. The curve on the top is Ω_0 when $\epsilon_{star} = 0$ and curves below it are $\Omega_0 - \frac{\kappa}{2}$ when $\epsilon_{star} = 0, 0.05, 0.1, 0.2, 0.3, 0.4, 0.5$. In our simulations $\epsilon_{star} = 0.1$, and in most part of the disk the rotation curve is very close to the one when $\epsilon_{star} = 0$. The difference is it reaches finite value instead of going infinite when $r \rightarrow 0$.

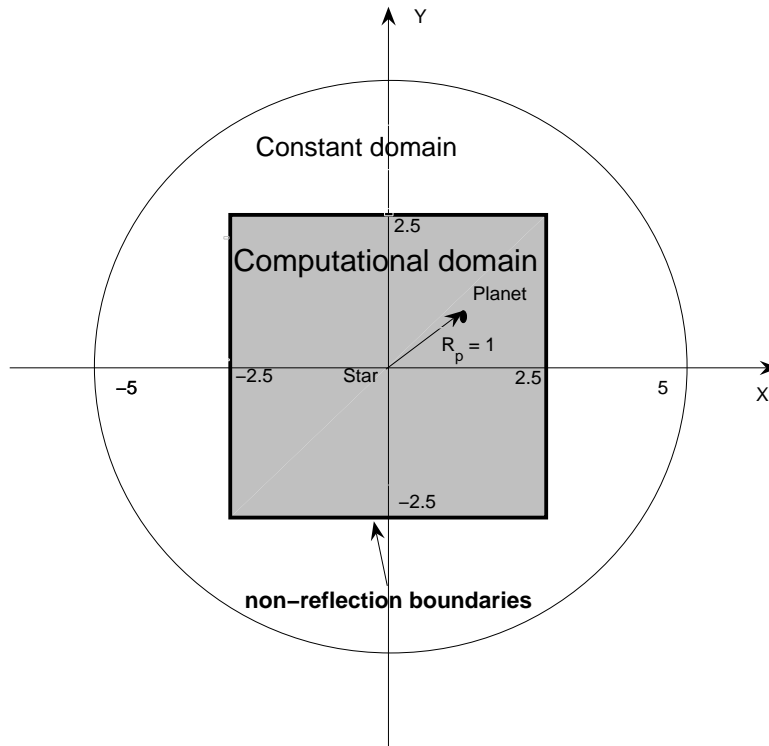


Fig. 2.— Computational domain. Computational domain is from -2.5 to 2.5 in x direction and from -2.5 to 2.5 in y direction(gray square). Surrounding it are four non-reflection boundaries. Area outside the square is assume to stay constant.

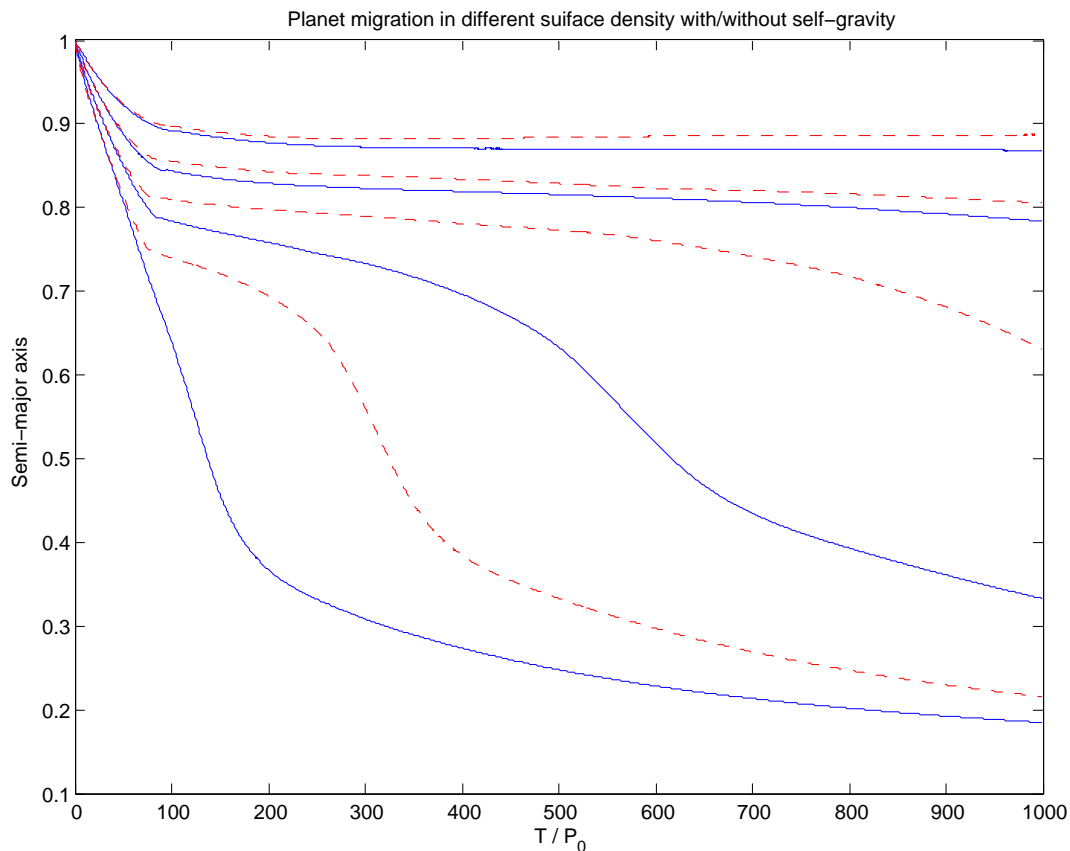


Fig. 3.— Migration in different disk surface density. From top to bottom, $\sigma = 0.6 \times 10^{-3}, 0.9 \times 10^{-3}, 1.2 \times 10^{-3}, 1.5 \times 10^{-3}$. MMSN mass corresponds to 0.6×10^{-3} in our units. The blue solid lines are the cases without self-gravity while the red dash lines denote the cases with self-gravity. The critical density to trigger runaway migration becomes higher in a self-gravitating disk.

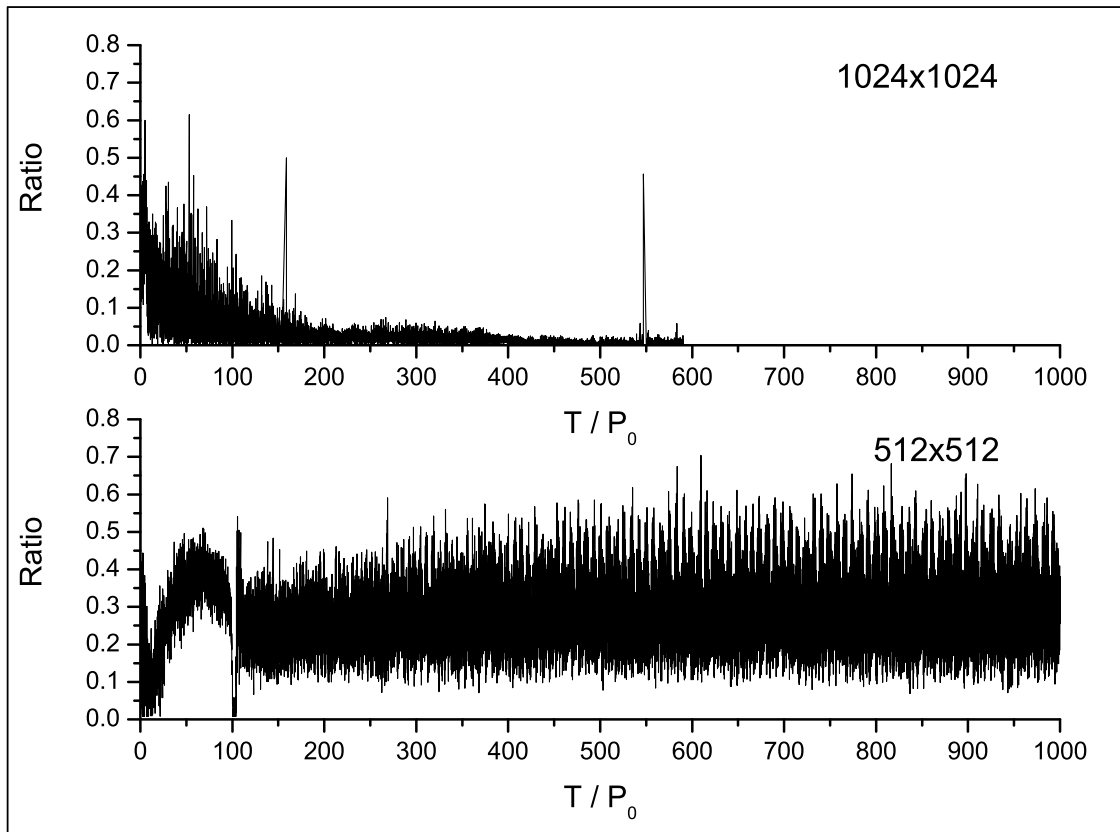


Fig. 4.— Ratio of torque(to planet) within planet’s Roche lobe to the torque(to planet) within the whole disk. The top one’s resolution is 1024×1024 and the bottom is of 512×512 . In the low resolution case the torque within planet’s Roche lobe is almost half of the whole torque during the simulation. And the rapid, large oscillations correspond to the unbalanced torque which is the consequence of mass flowing across unresolved vicinity of the planet. In high resolution case, the problem is not very serious.

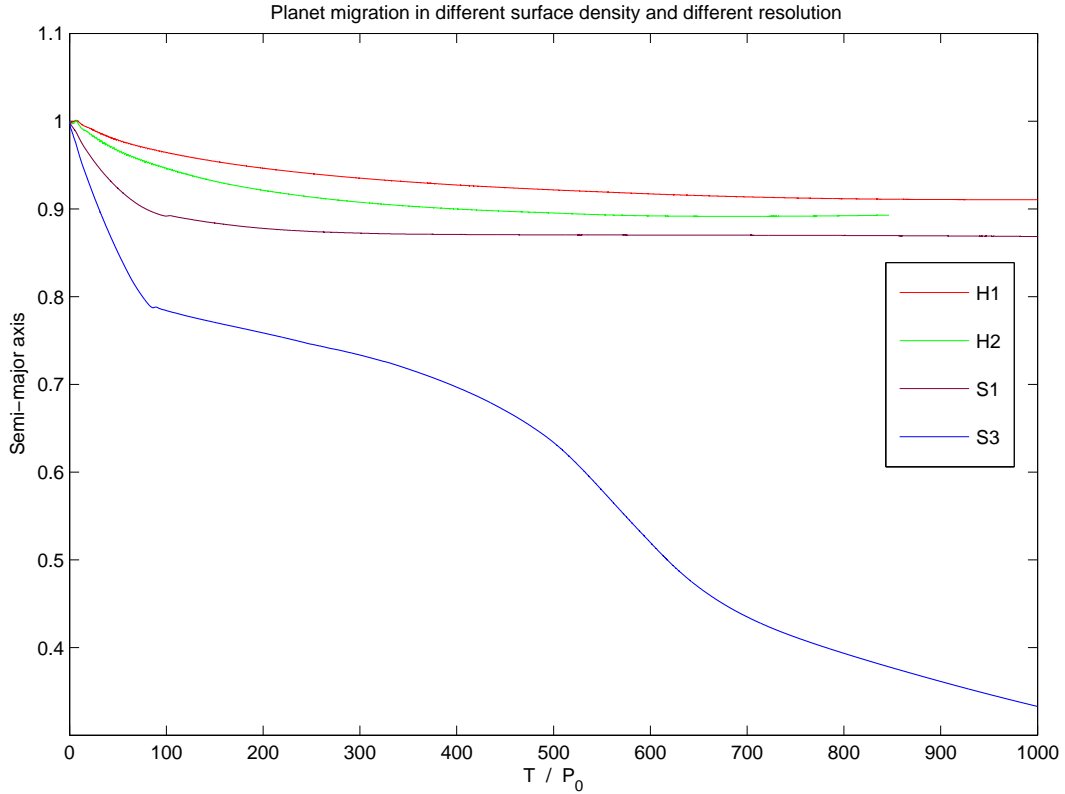


Fig. 5.— Migration curves. Red and green lines show the simulation in the resolution of 1024×1024 (H1 and H2) while the purple and blue lines are in the resolution of 512×512 (S1 and S3). The red and purple lines denote normal surface density $\sigma = 0.6 \times 10^{-3}$, the green and blue lines denote doubled surface density $\sigma = 1.2 \times 10^{-3}$. 'Runaway migration' occurs in low resolution case but doesn't show up in high resolution case although the surface density is the same.

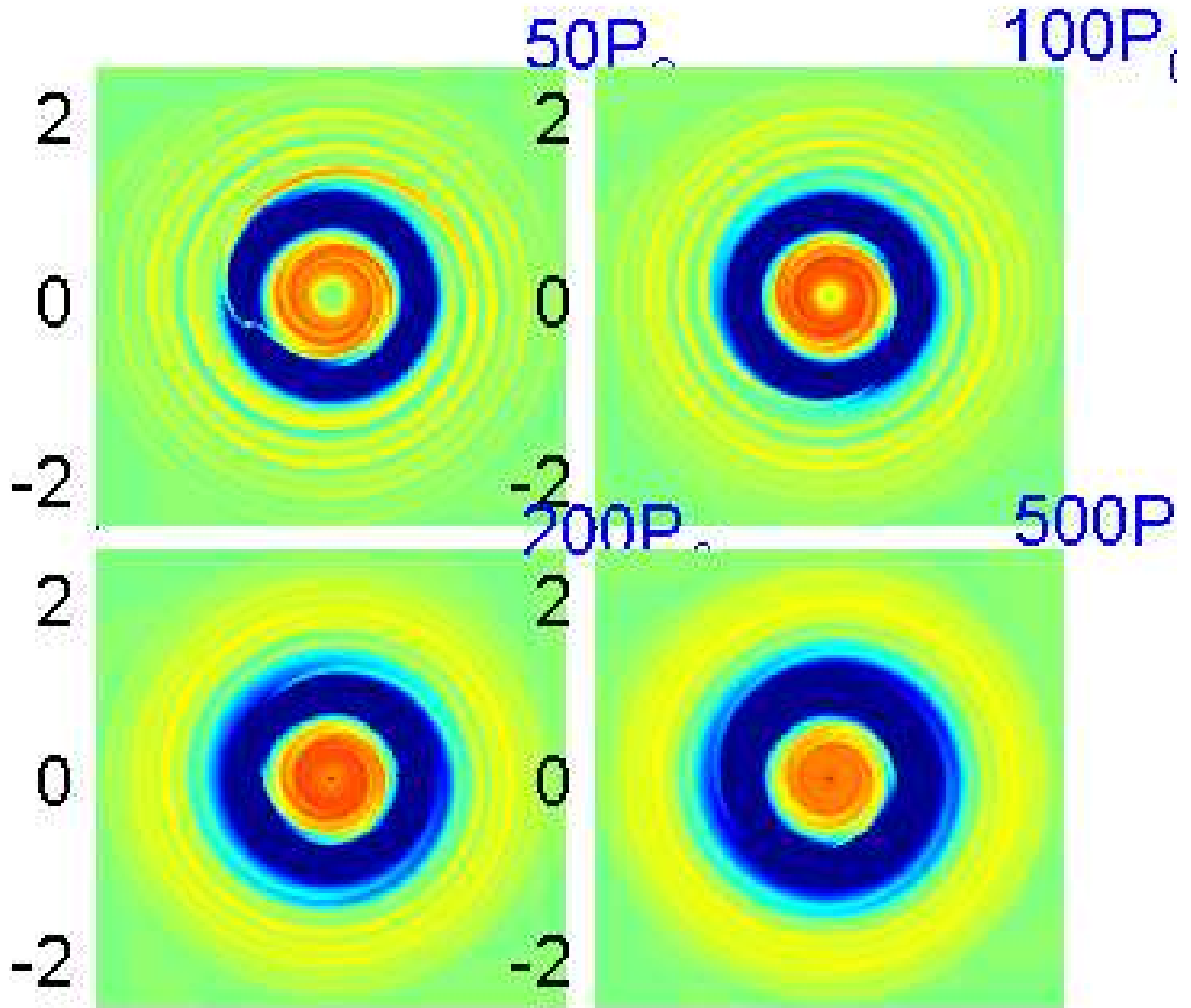


Fig. 6.— Density evolution of S3. The resolution is 512×512 and without self-gravity. From the top left to bottom right, evolution time is $50P_0$, $100P_0$, $200P_0$, $500P_0$.

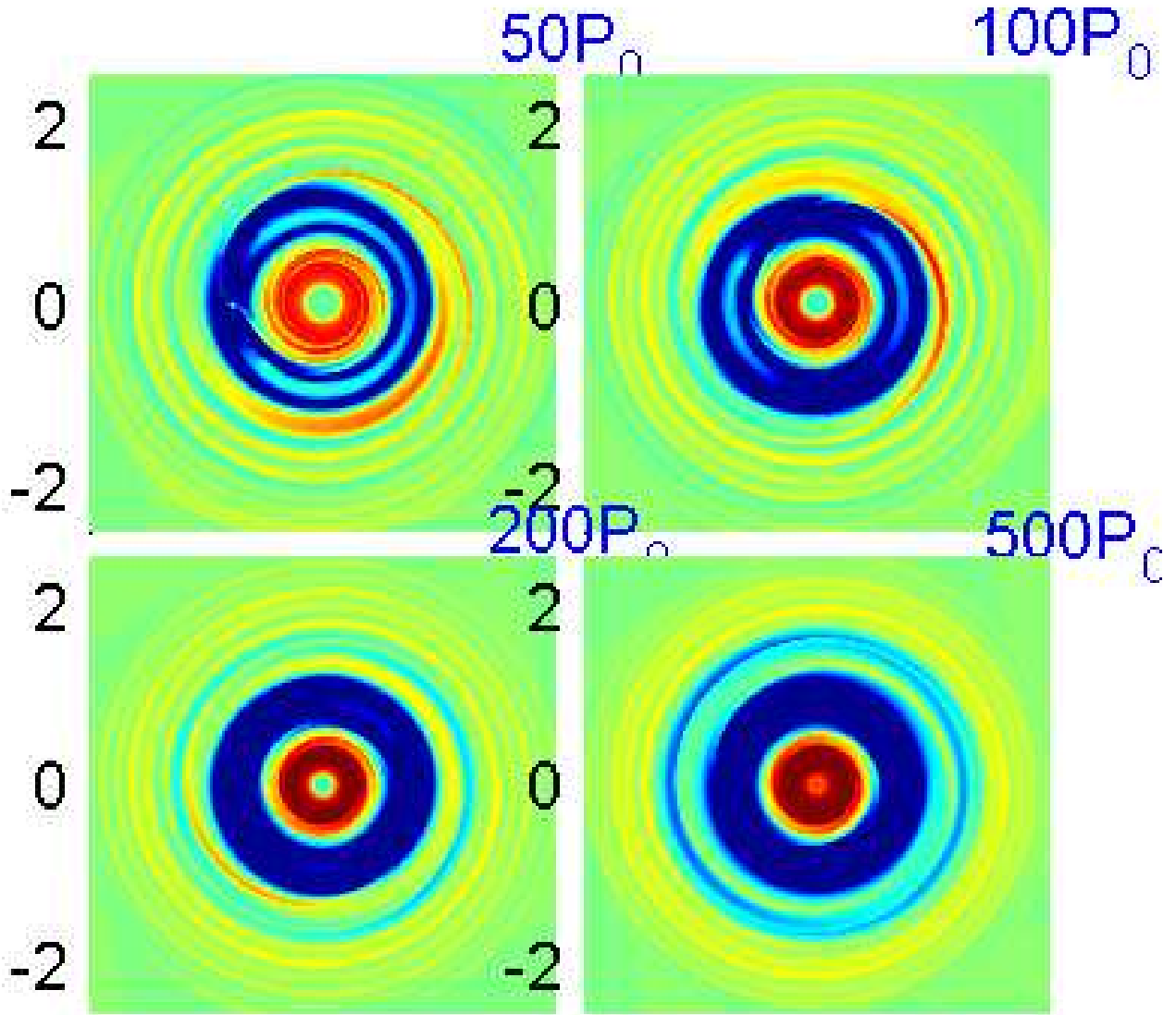


Fig. 7.— Density evolution of H₂. The resolution is 1024×1024 and without self-gravity. From the top left to bottom right, evolution time is $50P_0$, $100P_0$, $200P_0$, $500P_0$.

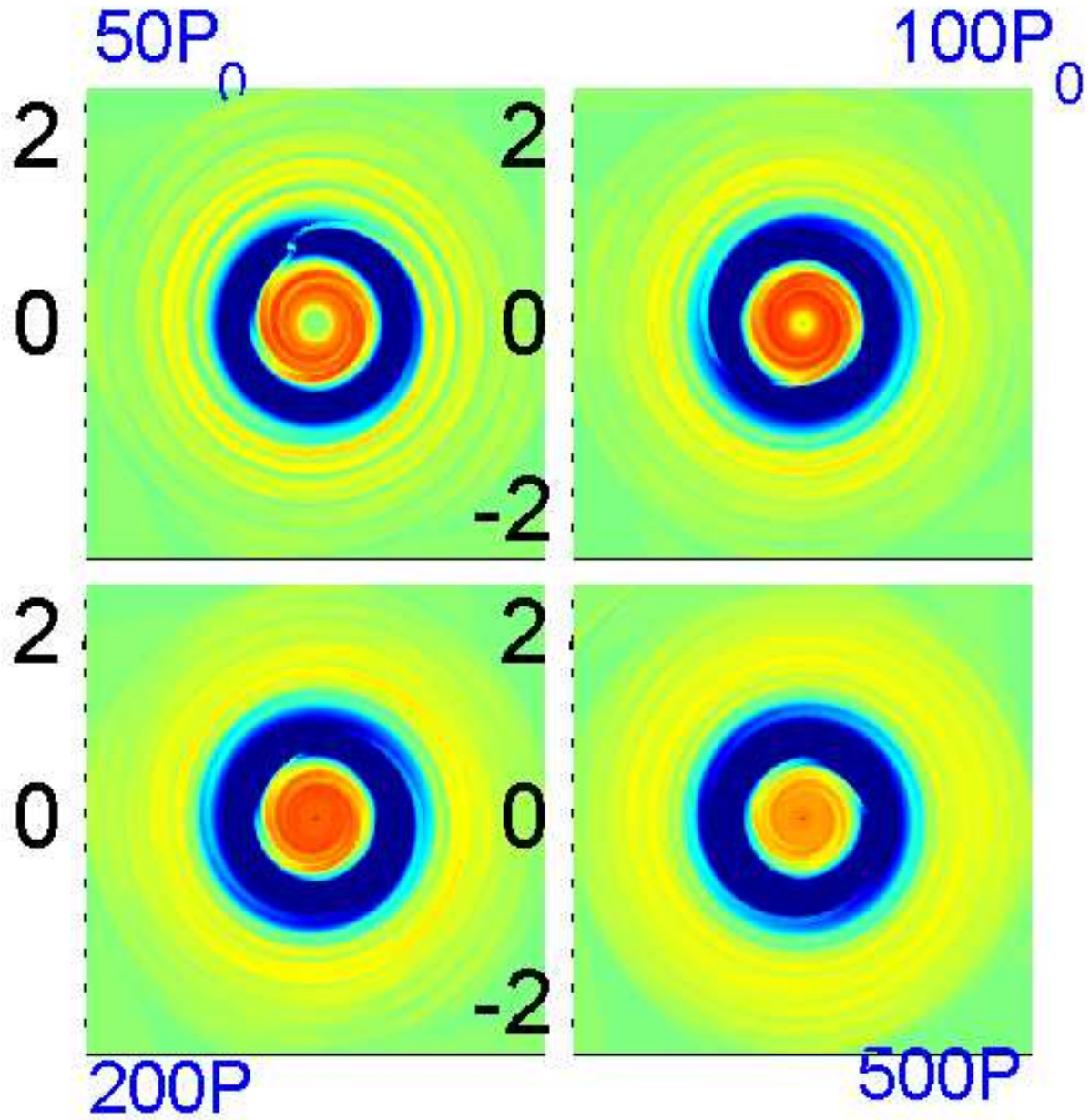


Fig. 8.— Density evolution of SG3. The resolution is 512×512 and self-gravitating effect is included. From the top left to bottom right, evolution time is $50P_0$, $100P_0$, $200P_0$, $500P_0$.

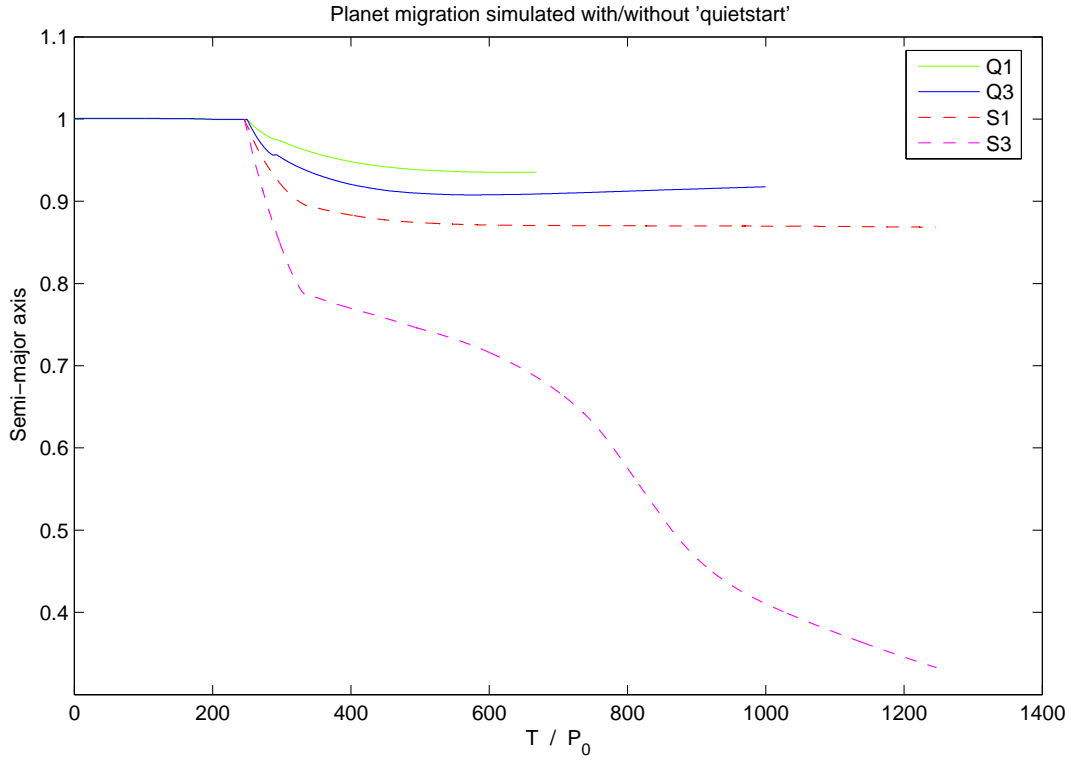


Fig. 9.— Migration with 'quiet start'. From top to bottom, the curve according to Q1,Q3,S1,S3. First $250P_0$ is 'quiet start' stage when the planet's orbit is fixed and planet grows gently.

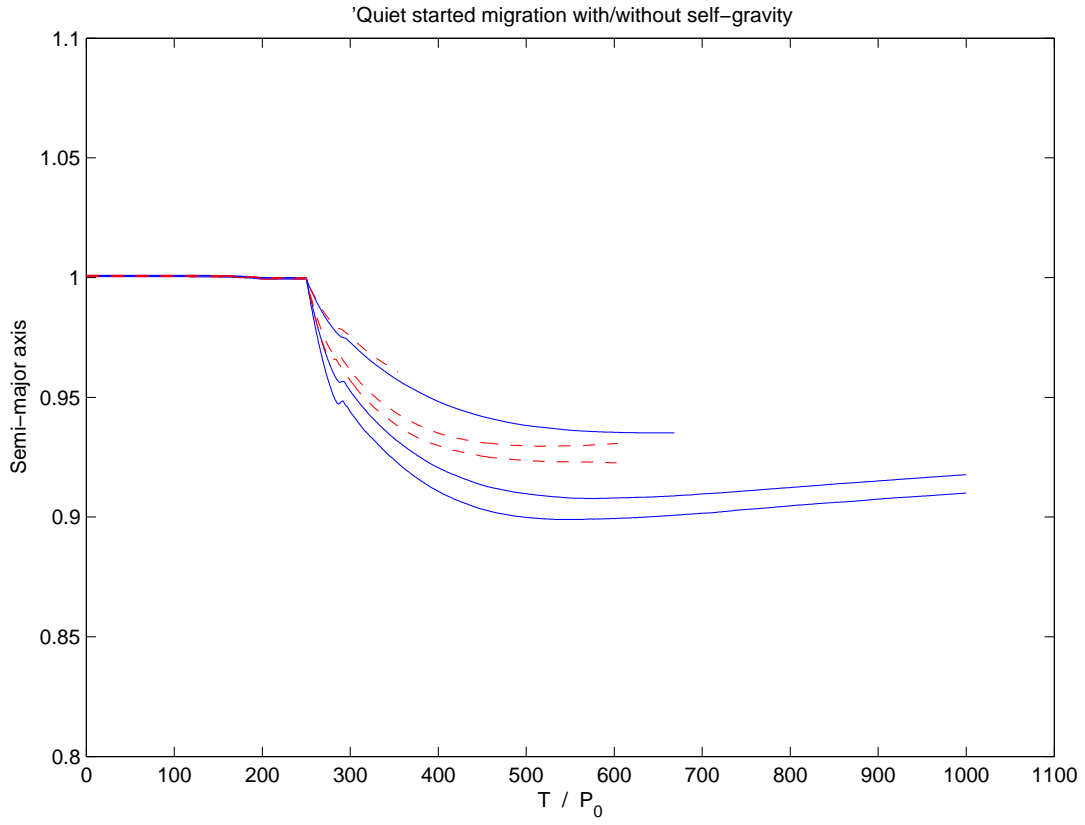


Fig. 10.— Migration in self-gravitating disk. From top to bottom, the three red dashed lines are QS1, QS3 and QS4 and the three blue solid lines are Q1, Q3 and Q4.

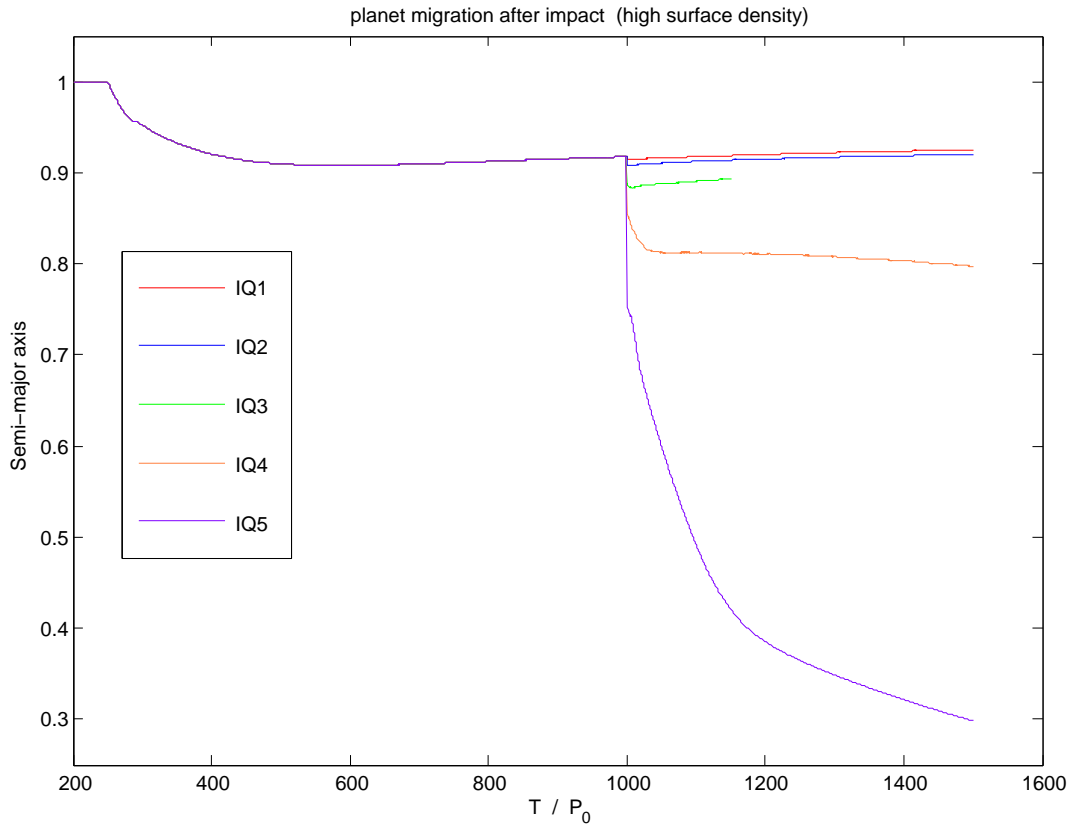


Fig. 11.— Migration after impact. It shows the migration curves after close encounters (IQ1-IQ5). 'Runaway migration' occurs when planet B is comparable to the A.

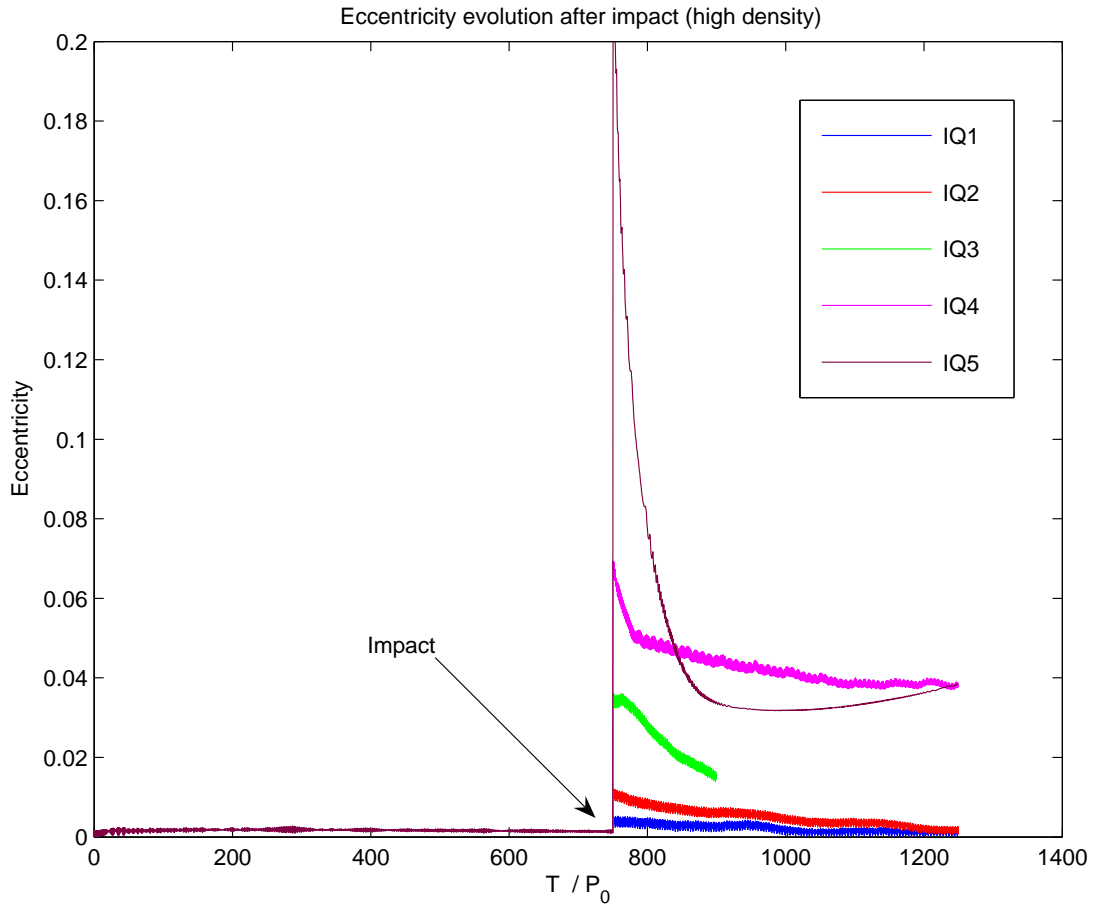


Fig. 12.— Eccentricity evolution after impact. It shows the eccentricity evolution after close encounters(IQ1-IQ5). The critical mass of the planet B which will break the steady state of planet A is of Saturn mass and the 'runaway migration' occurs when planet B is comparable to the A.

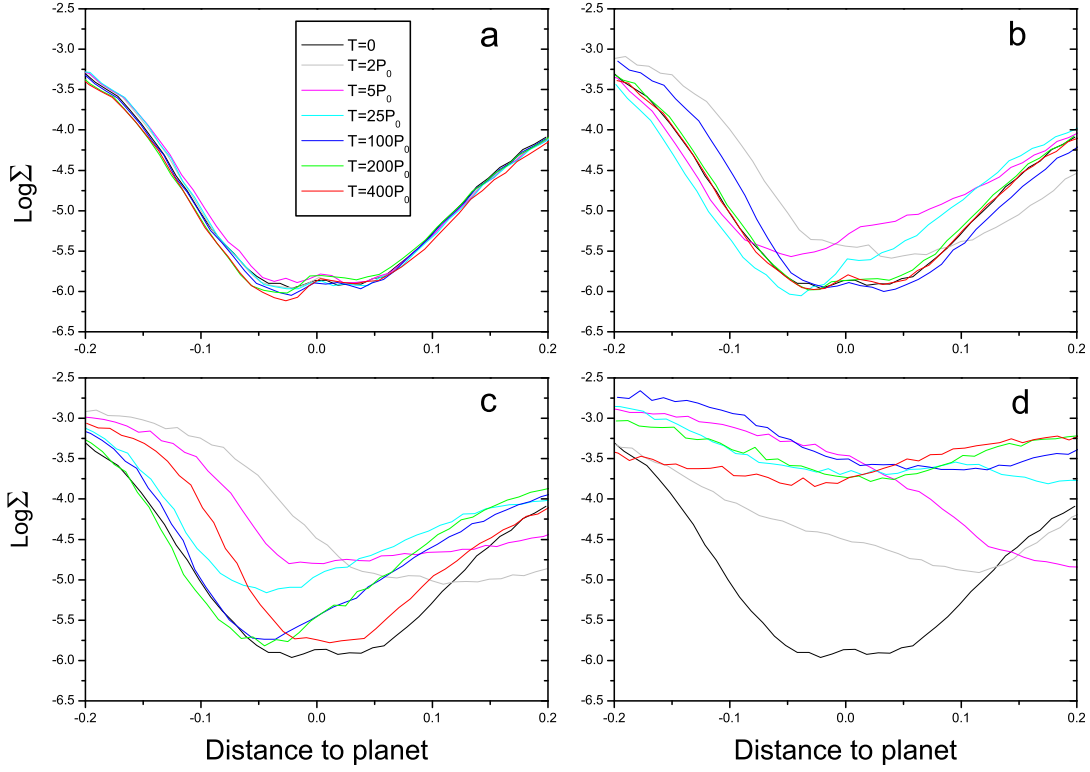


Fig. 13.— Logarithmic surface density distribution in the vicinity of planet A after close encounter. From the top left to the bottom right, figure a,b,c and d denote cases named IQ1,IQ3,IQ4 and IQ5 respectively. Results are in co-moving frame of planet A, X-axis is the distance to the planet A. The region is $(-3R_{Roche}, 3R_{Roche})$, where $R_{Roche} = 0.069$ is the initial Roche radius of planet A in our unit. Colored curves denote the different evolution time after close encounter: Black lines show the equilibrium state before close encounter. *a.* Planet A remains its equilibrium since density profile within planet’s vicinity doesn’t change much after small perturbation(IQ1 & IQ2). *b.* Gas floods into planet A’s vicinity short after relatively large perturbation(The gray lines) but depletes soon after $25P_0$ (The light green lines). So there is no runaway migration(IQ3). *c.* Gas takes about $400P_0$ to deplete(The red lines) in case IQ4 and planet A’s fast migration is suppressed finally since it can not self-sustained the vorticity gradient. *d.* Large radial perturbation allows planet A self-sustain the vorticity gradient in its vicinity. So it keeps losing angular momentum through the corotation resonance and under goes a run-away migration.